IIR GRAPPA for Parallel MR Image Reconstruction

Zhaolin Chen,[1,2,3]* Jingxin Zhang,[2] Ran Yang,[4] Peter Kellman,[5] Leigh A. Johnston,[1,3,6] and Gary F. Egan[1,7]

Accelerated parallel MRI has advantage in imaging speed, and its image quality has been improved continuously in recent years. This paper introduces a two-dimensional infinite impulse response model of inverse filter to replace the finite impulse response model currently used in generalized autocalibrating partially parallel acquisitions class image reconstruction methods. The infinite impulse response model better characterizes the correlation of *k*-space data points and better approximates the perfect inversion of parallel imaging process, resulting in a novel generalized image reconstruction method for accelerated parallel MRI. This *k*-space-based reconstruction method includes the conventional generalized autocalibrating partially parallel acquisitions class methods as special cases and has a new infinite impulse response data estimation mechanism for effective improvement of image quality. The experiments on in vivo MRI data show that the proposed method significantly reduces reconstruction errors compared with the conventional two-dimensional generalized autocalibrating partially parallel acquisitions method, particularly at the high acceleration rates. Magn Reson Med 63:502–509, 2010.

Key words: MRI; parallel imaging; accelerated imaging; GRAPPA; 2D GRAPPA; IIR GRAPPA

Parallel MRI is a technique that uses multiple receiver coils operating in parallel to acquire *k*-space signals. Because multiple receivers are used, the image acquisition can be accelerated several times compared to the conventional full *k*-space acquisition. Many image reconstruction methods have been developed in recent years to take full advantage of parallel MRI in different medical imaging applications. Of these methods, sensitivity encoding (SENSE) (1) and generalized autocalibrating partially parallel acquisitions (GRAPPA) (2) are the most widely used ones because of their simplicity and image reconstruction performance.

SENSE and GRAPPA represent two classes of methods with numerous extensions and variants for different applications. The SENSE class methods, also known as the image domain methods, include such methods as parallel imaging with localized sensitivities (3) and sensitivity profiles from an array of coils for encoding and reconstruction in parallel (4). The SENSE class methods compute the coefficients in the image domain. The GRAPPA class methods, also known as the *k*-space methods, include simultaneous acquisition of spatial harmonics (5), autocalibrating simultaneous acquisition of spatial harmonics (6), variable density autocalibrating-simultaneous acquisition of spatial harmonics (7), and the two-dimensional (2D) GRAPPA methods (8–10). While the calibration step in these methods, e.g., in simultaneous acquisition of spatial harmonics, may rely on the image domain coil sensitivities, the calculated coefficients are in *k*-space.

Compared with the *k*-space methods, the image domain methods normally require pre-estimated coil sensitivity profiles and then invert the sensitivity profiles to reconstruct an image. These methods can achieve an optimal reconstruction, provided the coil sensitivity profiles can be obtained precisely. However, the estimated sensitivity profiles often contain errors caused by noise, sensitivity misregistration, Gibbs ringing, and other estimation uncertainties (11,12), which reduce the final image reconstruction quality. Furthermore, the SENSE reconstructions are also limited in the field-of-view selections (13,14). The *k*-space methods avoid the explicit sensitivity estimation and inversion procedure by estimating directly an inverse filter (reconstruction model) using autocalibrating signals (ACS). The ACS are phase-encoding lines acquired at the Nyquist rate, with the phase-encoding gradient intervals set to satisfy the full field of view condition, which renders the *k*-space fitting of the inverse filter. Filtering the downsampled *k*-space signal through the inverse filter, the unacquired *k*-space data can then be estimated. This procedure is also known as the *k*-space fitting process.

The original GRAPPA method (2) used *k*-space fitting only along the phase encoding direction and was later extended to the *k*-space time domain (*k*-t) (15,16). The spatial 2D version of GRAPPA (8–10) extended the original GRAPPA fitting process to include both frequency and phase-encoding directions. It is equivalent to a 2D filtering and significantly improves the image quality. Despite the continuous improvement of image quality in accelerated parallel imaging over the last decade, image artifacts such as aliasing and noise are still quite obvious when compared with conventional full field-of-view acquisitions, especially at high acceleration rates.

Using the filter bank theory, the authors have recently analyzed the difficulties associated with parallel MR image reconstruction (11,17). It has been shown that the degraded

[1]Howard Florey Institute, Florey Neuroscience Institutes, Carlton, Victoria, Australia

[2]Department of Electrical and Computer Systems Engineering, Monash University, Clayton, Victoria, Australia

[3]Department of Electrical and Electronic Engineering, University of Melbourne, Parkville, Victoria, Australia

[4]School of Information Science and Technology Sun Yat-Sen University, Guangzhou, Guangdong, China

[5]Laboratory of Cardiac Energetics, NHLBI, NIH, DHHS, Bethesda, Maryland, USA

[6]NICTA Victorian Research Laboratory, Parkville, Victoria, Australia

[7]Centre for Neuroscience, University of Melbourne, Australia

*Correspondence to: Zhaolin Chen, PhD, Howard Florey Institute, Florey Neuroscience Institutes, 161 Barry Street, Carlton, VIC 3053, Australia. E-mail: zhaolin.chen@florey.edu.au

Received 23 December 2008; revised 7 July 2009; accepted 14 August 2009.
DOI 10.1002/mrm.22197
Published online 26 October 2009 in Wiley InterScience (www.interscience.wiley.com).

image quality is partially due to the use of suboptimal reconstruction models in current reconstruction methods. Therefore, the development of optimal reconstruction models presents an important direction for further improvement of image quality. Based on these analysis results, this paper introduces a 2D infinite impulse response (IIR) model of inverse filter to replace the finite impulse response (FIR) model currently used in the GRAPPA class methods. It will be shown that the proposed model captures more precisely the correlation of k-space data points and approximates more closely the perfect inversion of parallel imaging process. Using the proposed model, a new generalized image reconstruction method is presented for accelerated parallel MRI and compared mathematically and experimentally with the conventional GRAPPA to demonstrate its advantages in reducing reconstruction errors.

THEORY

Linear System View of Parallel MRI Reconstruction

An L-receive coil Fourier encoded MRI process is defined as

$$s_l(k_y,k_x)=\sum_{n_y=0}^{N_{pe}-1}\sum_{n_x=0}^{N_{fe}-1} C_l(n_y,n_x)P(n_y,n_x)\exp\left\{j\frac{2\pi}{N_{pe}}k_y n_y\right\} \times\exp\left\{j\frac{2\pi}{N_{fe}}k_x n_x\right\},\quad 0\le k_y\le N_{pe}-1,\ 0\le k_x\le N_{fe}-1, \tag{1}$$

where $s_l(k_y,k_x)$ is the lth coil received k-space signal. Function $C_l(n_y,n_x)$ represents the sensitivity profile of the lth channel, and $P(n_y,n_x)$ is the image function that is digitized by the encoding process. The values N_{fe} and N_{pe} are the total numbers of frequency-encoding and phase-encoding steps in a full field of view, respectively. The variables k_y and k_x are k-space indices along the phase- and frequency-encoding directions, and the variables n_y and n_x are spatial indices in the image domain along the vertical and horizonal directions.

By the circular convolution theorem (18), for the 2D discrete Fourier transform, Eq. 1 can be represented by a convolution operator $\Gamma_l : p \mapsto s_l$, which is the imaging operator and defined as

$$\Gamma_l:\quad s_l(k_y,k_x)=c_l(k_y,k_x)*p(k_y,k_x), \tag{2}$$

where $*$ denotes the 2D convolution operation, and $c_l(k_y,k_x)$ and $p(k_y,k_x)$ are the 2D Fourier transforms of $C_l(n_y,n_x)$ and $P(n_y,n_x)$ given, respectively, by

$$c_l(k_y,k_x)=\sum_{n_y=0}^{N_{pe}-1}\sum_{n_x=0}^{N_{fe}-1} C_l(n_y,n_x)\exp\left\{j\frac{2\pi}{N_{pe}}k_y n_y\right\} \times\exp\left\{j\frac{2\pi}{N_{fe}}k_x n_x\right\},$$

$$p(k_y,k_x)=\sum_{n_y=0}^{N_{pe}-1}\sum_{n_x=0}^{N_{fe}-1} P(n_y,n_x)\exp\left\{j\frac{2\pi}{N_{pe}}k_y n_y\right\} \times\exp\left\{j\frac{2\pi}{N_{fe}}k_x n_x\right\}.$$

In the systems theory context, Eq. 2 is a 2D single-input multioutput system, with input signal $p(k_y,k_x)$, output signal $s_l(k_y,k_x)$, and the system impulse response $c_l(k_y,k_x)$.

The above discussion describes the parallel imaging without accelerated acquisition. In an M-fold accelerated imaging and acquisition, k-space data are acquired every M phase lines. The signal thus acquired in each channel is given by

$$s_l(Mk_y,k_x)\triangleq s_l(k_y,k_x)\downarrow_M = c_l(k_y,k_x)*p(k_y,k_x)\downarrow_M, \tag{3}$$

where $\downarrow_M$ denotes the M-fold downsampling operator, with $M\ge 1$ being integer and $0\le Mk_y\le N_{pe}-M$.

The objective of image reconstruction is to find a function that maps the acquired (downsampled) k-space data $s_l(Mk_y,k_x)$, $l=1,\ldots,L$, from all channels to a desired complete set of k-space input data $p(k_y,k_x)$. Kholmovski and Samsonov (19) cast the GRAPPA reconstruction into an inverse operation of Eq. 3, and the difference of SENSE and GRAPPA was discussed from the inverse operator perspective (20).

2D GRAPPA

Denote Ψ_l the inverse operator in the GRAPPA class methods that maps the downsampled $s_l(Mk_y,k_x)$ from all the channels to a complete set estimated $s_l(k_y,k_x)$ of an individual channel. Mathematically, Ψ_l is defined as (2,9)

$$\Psi_l:\ \hat{s}_l(Mk_y-m,k_x) =\sum_{j=1}^{L}\sum_{b=-N_b}^{N_a}\sum_{h=-H_b}^{H_a} g_{l,m}(j,b,h)s_j(M(k_y-b),k_x-h), \tag{4}$$

$$N_a,N_b,H_a,H_b\ge 0,\quad m=1,\ldots,M-1,$$

where $g_{l,m}(j,b,h)$ are the coefficients of a fitting kernel, N_b and N_a define the size of the kernel along the phase-encoding direction, and H_b and H_a define the kernel size along the frequency-encoding direction. For $H_b=H_a=0$, Eq. 4 gives the original GRAPPA (2); otherwise, it represents the 2D GRAPPA methods (8,9).

As detailed elsewhere (2,9), the coefficients $g_{l,m}(j,b,h)$ are pre-estimated from a set of ACS (2), by using standard estimation methods such as the least squares algorithm, and are used in Eq. 4 to compute $\hat{s}_l(Mk_y-m,k_x)$ for $m=1,\ldots,M-1$. The computed $\hat{s}_l(Mk_y-m,k_x)$ are then combined with the acquired dataset $s_l(Mk_y,k_x)$ to form an estimate of the complete k-space data $\hat{s}_l(k_y,k_x)$ for each channel, with $\hat{s}_l(Mk_y,k_x)=s_l(Mk_y,k_x)$. The $\hat{s}_l(k_y,k_x)$ thus obtained are taken as an estimate of $p(k_y,k_x)$ from the lth coil, denoted as $\hat{p}_l(k_y,k_x)$ below.

$$\hat{p}_l(k_y,k_x)=\hat{s}_l(k_y,k_x). \tag{5}$$

The 2D Fourier transform of $\hat{p}_l(k_y, k_x)$ gives the subimage $\hat{P}_l(n_y, n_x)$ from the lth coil, and the square root sum of squares of subimages $\hat{P}_l(n_y, n_x)$ from all the coils is used to reconstruct a final image, given as $\hat{P}(n_y, n_x) = \sqrt{\sum_l^L \hat{P}_l^2(n_y, n_x)}$.

From Eqs. 3, 4 and 5, it is evident that Ψ_l given in Eq. 4 functions as an inverse operator that maps the downsampled $s_l(Mk_y, k_x)$ from all the channels to a complete set estimated $s_l(k_y, k_x)$ of an individual channel, and then to the estimated $P_l(n_y, n_x)$ of the channel. Further, Eq. 4 clearly shows that the inverse operators Ψ_l in GRAPPA are in fact the 2D FIR filters in the terminology of systems and signals because the structure of Eq. 4 is analogous to the structure of FIR filter function, or the 2D moving average (MA) estimators in the terminology of statistical analysis (18). For this reason, Ψ_l will also be referred to as an inverse filter in the sequel.

IIR GRAPPA

Using the filter bank theory, the authors have recently analyzed the difficulties in image reconstruction of parallel MRI (11,17). It is shown that the FIR or equivalently the MA structure in the inverse filter Eq. 4 is a major reason for the degraded image quality. To overcome this difficulty, the following new structure is proposed for the inverse filter used in GRAPPA class methods:

$$\begin{aligned}\Psi_l:\ \hat{s}_l(Mk_y - m, k_x) &= \sum_{j=1}^{L}\sum_{q=-Q_b}^{Q_a}\sum_{r=-R_b}^{R_a} a_{l,m}(j,q,r)\hat{s}_j(Mk_y - m - q, k_x - r) \\ &+ \sum_{j=1}^{L}\sum_{b=-N_b}^{N_a}\sum_{h=-H_b}^{H_a} g_{l,m}(j,b,h)s_j(M(k_y - b), k_x - h), \quad [6]\end{aligned}$$

$$m = 1, \ldots, M-1,\ Q_a, Q_b, H_a, H_b, N_a, N_b, H_a, H_b \geq 0,$$

$$a_{l,m}(j,0,0) = 0,\ \hat{s}_l(Mk_y, k_x) = s_l(Mk_y, k_x).$$

Compared with Eq. 4, the proposed structure has a new part that represents the linear dependence of the current estimates on the "previous (neighboring)" estimates, with its structure controlled by the values of Q_b, Q_a, R_b, and R_a. When either Q_b or Q_a is chosen as zero, this new part becomes (causal or anticausal) autoregression (AR) of the estimate $\hat{s}_l(Mk_y - m, k_x)$, which, together with the original MA part in Eq. 4 constitutes a 2D autoregression moving average (ARMA) estimator of the unacquired k-space data $s_l(Mk_y - m, k_x)$. When Q_b and Q_a are both nonzero, Eq. 6 becomes a noncausal 2D filter. The values of Q_b and Q_a define the order of the AR part in the phase-encoding direction, and R_b and R_a are the order of the AR part in the frequency-encoding direction. Similarly to the conventional GRAPPA, the kernel coefficients $a_{l,m}(j,q,r)$ and $g_{l,m}(j,b,h)$ can be obtained by using ACS lines and standard parameter estimation methods such as the regularized least squares algorithm (21).

As a filter, Eq. 6 has an IIR when $Q_b \neq 0$ and/or $Q_a \neq 0$. This may be understood by considering an impulse function as the input, Eq. 6 will result in the output that will have an infinite length of response. Thus, it gives rise to a new reconstruction method named IIR GRAPPA in this paper. For $Q_b = Q_a = R_b = R_a = 0$, Eq. 6 reduces to Eq. 4. Therefore, IIR GRAPPA is a generalized reconstruction method that includes original GRAPPA (2) and 2D GRAPPA (8,9) as special cases.

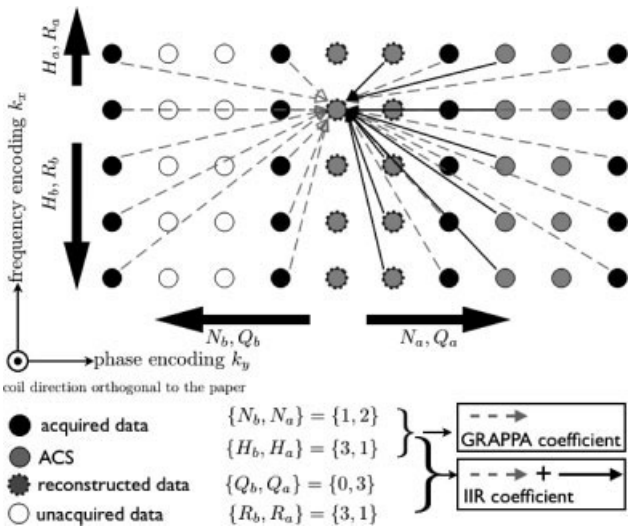

FIG. 1. Comparison of GRAPPA and IIR GRAPPA in a 3-fold accelerated imaging example. Vertical direction is the frequency-encoding direction, and the horizontal direction is the phase-encoding direction. The coil direction is perpendicular to the paper. The dashed arrows are the fitting coefficients of a 2D GRAPPA method; the dashed plus solid arrows are the fitting coefficients of an IIR GRAPPA method.

Figure 1 shows a 3-fold accelerated imaging example for a visual comparison of the difference between IIR GRAPPA and 2D GRAPPA. As seen from the figure, 2D GRAPPA uses only the acquired data to reconstruct (estimate) the unacquired data, while IIR GRAPPA uses both the acquired and estimated data in reconstruction. As analyzed and experimentally demonstrated in the Discussion and Results sections, this key difference renders IIR GRAPPA a better reconstruction performance.

Because IIR GRAPPA uses the estimated data in reconstruction, the initial values of these estimates are needed in order to use the AR part in Eq. 6. There are in general two approaches to obtain initial values. The first approach is the "one-step" approach, which uses directly the data in ACS lines (normally in the center of the k-space) as the initial values. In this case, the reconstruction of the left half of the k-space as shown in Fig. 1 should have $Q_b = 0$ because all the available ACS data are on its right side (from the reader's view direction). Similarly, $Q_a = 0$ should be used for the right half of the k-space. The other approach is the "two step" approach. In this approach, the MA fitting is first done to obtain initial estimates of unacquired k-space data. With these estimated initial values, the AR filtering can then be performed to obtain the final reconstruction. In this two-step approach, Q_a and Q_b can be chosen as nonzero values for the reconstruction of the both sides of k-space.

MATERIALS AND METHODS

Data Acquisitions

A brain imaging dataset was acquired to test the performance of the proposed method for high-resolution brain-imaging applications. The *k*-space data were acquired from a Siemens Tim Trio 3T system with a Siemens 12-channel head matrix coil (Siemens Medical Solutions, Erlangen, Germany). The imaging parameters were as follows: axial 2D gradient recall echo, T_2^*-weighted imaging with echotime = 45 ms, pulse repetition time = 1000 ms approximate, flip angle = 45°, slice thickness = 2.5 mm, field of view = 240 mm × 180 mm, $N_{fe} = 448$, $N_{pe} = 384$. Full *k*-space data were acquired for each channel and were then manually uniformly downsampled to simulate 3- and 4-fold accelerated imaging. The ACS lines were chosen at the 64 (16.67% N_{pe}), 48 (12.50% N_{pe}) and 32 (8.33% N_{pe}) locations in the central *k*-space.

Evaluation of Reconstruction Methods

The 2D GRAPPA (8,9) and IIR GRAPPA algorithms were both implemented in the Matlab programming environment (Mathworks, Natick, MA) for comparison. For both methods, the subimages are combined with the square root sum of squares method. The full field of view reference image I^{ref} without accelerated imaging was calculated using square root of sum of squares of all of the receiver coil images. The root mean squared (RMS) error of a reconstructed image was calculated from

$$\text{RMS} = \sqrt{\frac{1}{N_{fe} \times N_{pe}} \sum_{i=1}^{N_{pe}} \sum_{j=1}^{N_{\text{fe}}} \frac{\left| I_{i,j}^{recon} - I_{i,j}^{\text{ref}} \right|^2}{\left| I_{i,j}^{ref} \right|^2}} \qquad [7]$$

where $\{i, j\}$ are pixel indices. The reconstruction error (ERR) image was calculated from

$$\text{ERR} = |I^{recon} - I^{ref}| \qquad [8]$$

which is the absolute difference between a reconstructed image and the reference image.

Determination of Reconstruction Kernel Size

The reconstruction kernel size was determined by comparing the RMS errors of reconstruction under different kernel sizes. A larger kernel size generally results in less reconstruction error, but it increases the kernel complexity and requires more kernel coefficients. As a result, more ACS data are required to obtain a decent estimate of the kernel coefficients, and more time is needed to estimate the coefficients and to reconstruct the unacquired *k*-space data. This may be understood from solving overdetermined systems perspective. With increased numbers of unknowns, more equations are generally required to obtain an accurate and robust solution. A tradeoff is thus always necessary. To select the reconstruction kernels for our experiments, 2D GRAPPA and IIR GRAPPA were evaluated under different kernel sizes, using a 3-fold accelerated acquisition with 12% ACS lines of the above acquired data.

As shown in Eq. 6, the kernel size in IIR GRAPPA is jointly determined by the size of the IIR (AR) part $(Q_a+Q_b)\times(R_a+R_b)$ and the size of the MA part $(N_a+N_b)\times(H_a+H_b)$, while in 2D GRAPPA it is determined only by the size of the MA part $(N_a + N_b) \times (H_a + H_b)$. To make a meaningful comparison, these two methods were evaluated against different sizes of $(N_a + N_b) \times (H_a + H_b)$, and for each $(N_a + N_b) \times (H_a + H_b)$, the corresponding size of the IIR part, $(Q_a+Q_b)\times(R_a+R_b)$, in IIR GRAPPA was constrained to be $(Q_a + Q_b) \times (R_a + R_b) \leq (N_a + N_b) \times (H_a + H_b)$. Thus, the two methods were compared under the condition that they both use the same number of acquired data points in reconstruction, which is equal to the size $(N_a + N_b) \times (H_a + H_b)$.

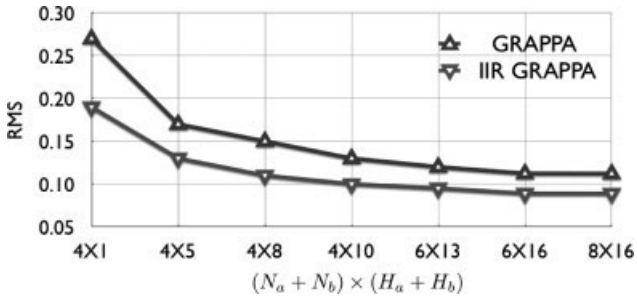

FIG. 2. Comparison of reconstruction errors of 2D GRAPPA and IIR GRAPPA in a 3-fold accelerated acquisition under different MA size $(N_a + N_b) \times (H_a + H_b)$. For IIR GRAPPA, the size of IIR part was constrained to be $(Q_a + Q_b) \times (R_a + R_b) \leq (N_a + N_b) \times (H_a + H_b)$.

By considering both reconstruction errors (presented in Fig. 2 of the Results section) and computation complexity, the following kernel sizes were selected for the experiments to evaluate the optimum between image quality, robustness, and computational expense: For 2D GRAPPA, the MA part was $(N_a+N_b)\times(H_a+H_b) = 4\times10$; for IIR GRAPPA, the MA part was the same as 2D GRAPPA, and the IIR part was $(Q_a+Q_b)\times(R_a+R_b) = 3\times10$, which satisfies the condition $(Q_a + Q_b) \times (R_a + R_b) \leq (N_a + N_b) \times (H_a + H_b)$.

Regularized Least Squares Algorithm

As commonly used in practice, the regularized least squares algorithm was implemented in both 2D GRAPPA and IIR GRAPPA to obtain the kernel coefficients. The truncated singular value decomposition (SVD) approach (21) described in the Appendix was adopted, and the regularization threshhold was empirically chosen by observing the RMS reconstruction errors of both methods with different kernel sizes.

Initial Values in Reconstruction

For simplicity, the one-step approach as described in Theory section was used throughout the experiments to obtain the initial values in reconstruction. This was based on the observation that for the acquired dataset, no significant difference was observed from using the two-step approach.

RESULTS

Reconstruction Error Under Different Kernel Sizes

Figure 2 shows the RMS reconstruction errors of 2D GRAPPA and IIR GRAPPA under different kernel sizes. As

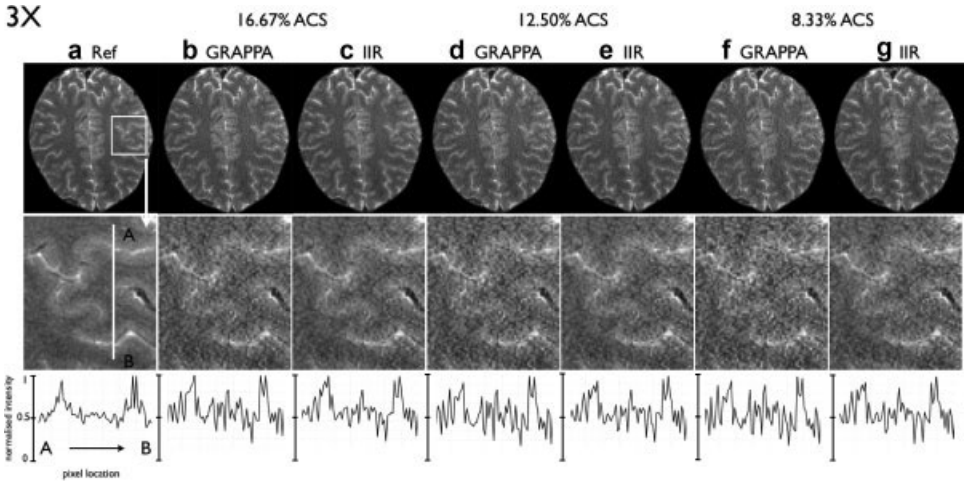

FIG. 3. Reconstructed images of 2D GRAPPA and IIR GRAPPA using the 3-fold accelerated imaging. For 2D GRAPPA, $(N_a+N_b)\times(H_a+H_b) = 4\times10$, and for IIR GRAPPA, $(N_a+N_b)\times(H_a+H_b) = 4\times10$ and $(Q_a+Q_b)\times(R_a+R_b) = 3\times10$. **a**: The reference image; (**b-g**) the reconstructed images using a different percentage of ACS lines. The second row shows corresponding enlarged regions in the inset box from the top panel. The last row plot line profiles from A to B of each image. Images are shown in the same grayscales.

seen from the plots, the errors for both methods decrease dramatically as the MA size $(N_a+N_b)\times(H_a+H_b)$ increases from 4×1 to 4×10. However, as the kernel size further increases, the reconstruction errors for both methods decrease slowly and tend to stabilize at different minimum values when extremely large kernel sizes are used. It is evident that with all the MA sizes, or equivalently with the same numbers of acquired data points, IIR GRAPPA produces considerably fewer reconstruction errors than 2D GRAPPA does. With significantly larger MA size, 2D GRAPPA may be able to match the performance of IIR GRAPPA at some smaller MA sizes, e.g., the performance of 2D GRAPPA at the MA size 8×16 is close to that of IIR GRAPPA at the MA size 4×8. However, with all the MA sizes tested, 2D GRAPPA is unable to match the minimal error achieved by IIR GRAPPA at the MA size 8×16.

Impact of Regularization Threshold

For the truncated SVD regularization described in the Appendix, the regularization threshold was empirically chosen as 0.5×10^{-3} for both 2D GRAPPA and IIR GRAPPA methods. With further increase of the threshold, strong aliasing was observed and the RMS error plots in Fig. 2 showed an "U" shape, as described in Nana et al. (22), for both methods. This indicates that if the kernel size and regularization threshold are both large, the estimation of kernel coefficients will be too poor to use for either method. Nevertheless, it was observed that the IIR GRAPPA method showed consistently less reconstruction error at different levels of regularization, except when a very large regularization threshold was used, and no difference was observed between the two methods.

Comparison of Reconstructed Images

The dataset in this experiment uses a long echo time, which reduces the inherent signal to noise ratio (SNR) in each sampled voxel and enables an evaluation of the performance of reconstruction algorithms. Both 3-fold (Fig. 3) and 4-fold (Fig. 4) accelerated acquisitions were used with varying ACS lines. In both figures, the IIR GRAPPA images have significantly improved overall image quality compared with the 2D GRAPPA images. The improved image quality can be observed clearly in the enlarged views and the plotted line profiles crossing two cortical regions. The IIR GRAPPA method has significantly reduced overall RMS errors in the reconstructed images (Figs. 5 and 6).

For the group of 3-fold acceleration (Fig. 3), the IIR GRAPPA image using 16.67% N_{pe} as ACS shows the best reconstruction quality throughout the image (Fig. 3c). With other numbers of ACS lines, the IIR GRAPPA images consistently provide noticeable reduction in reconstruction errors (i.e., noise + aliasing artifacts) when compared with its 2D GRAPPA counterparts. Consider the line profile from point A to point B, which traverses two cortical areas (high intensity) and a white matter area (low intensity). As can be observed in the pixel intensity against pixel location plots, all images using 3-fold acceleration identify the peaks (i.e., the cerebrospinal fluid and surrounding gray matter). In the low-signal white matter regions (the middle area in the plots), both reconstruction methods produce increased signal variance caused by reconstruction errors; however, less fluctuation is observed in the IIR GRAPPA plots. Therefore, the images produced by IIR GRAPPA have clearer and more traceable cortical structures than those by GRAPPA.

The advantage is even more pronounced for a 4-fold acceleration (Fig. 4). The maximum acceleration occurs when as few as only 8.33% ACS lines are used (Fig. 4e,f). In this situation, the 2D GRAPPA image (Fig. 4e) fails to show the cortical structures and white matter areas as seen in both the enlarged view and the line plot, while in the IIR GRAPPA image (Fig. 4f), the major tracks of cortical regions are still evident. For other images, the IIR GRAPPA images clearly show less reconstruction error than the 2D GRAPPA images.

The reconstruction error images (Fig. 5) and the overall RMS comparison (Fig. 6) show the difference between the reconstruction errors of 2D GRAPPA and IIR GRAPPA.

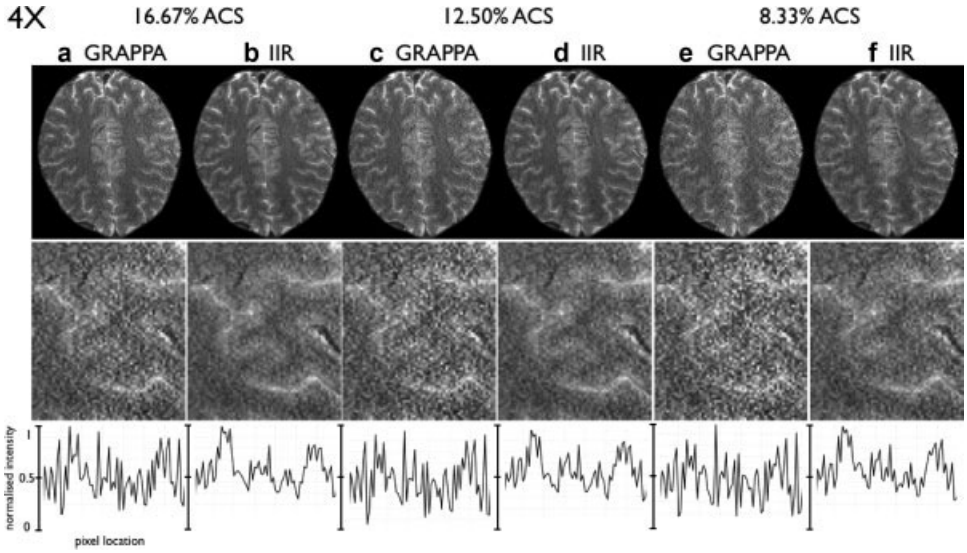

FIG. 4. Reconstructed images of 2D GRAPPA and IIR GRAPPA using 4-fold accelerated imaging. For 2D GRAPPA, $(N_a + N_b) \times (H_a + H_b) = 4 \times 10$, and for IIR GRAPPA, $(N_a + N_b) \times (H_a + H_b) = 4 \times 10$ and $(Q_a + Q_b) \times (R_a + R_b) = 3 \times 10$. The first row is the reconstructed images using a different percentage of ACS lines. The second row shows the enlarged regions in the inset box. The last row shows the line profiles, as indicated in Fig. 3a. Images are shown in the same grayscales.

The difference is more noticeable as the acceleration factor increases and the number of ACS lines decreases. This pattern is expected because an IIR filter can use fewer data to approximate a relatively complex system compared with an FIR filter.

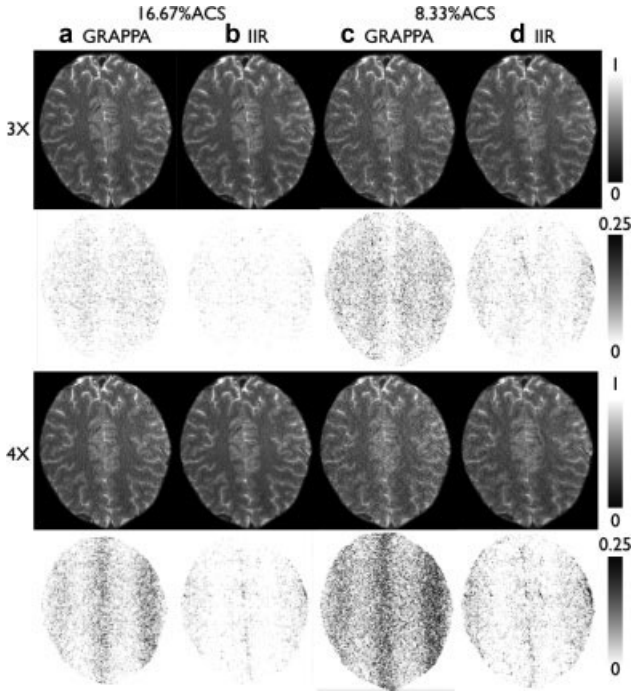

FIG. 5. Reconstruction error images of 2D GRAPPA and IIR GRAPPA. For 2D GRAPPA, $(N_a + N_b) \times (H_a + H_b) = 4 \times 10$, and for IIR GRAPPA, $(N_a + N_b) \times (H_a + H_b) = 4 \times 10$ and $(Q_a + Q_b) \times (R_a + R_b) = 3 \times 10$. **a,b**: GRAPPA and IIR GRAPPA using 16.67% ACS lines, respectively; (**c,d**) GRAPPA and IIR GRAPPA using 8.33% ACS lines, respectively. The second and the fourth rows are error images.

DISCUSSION

The above experiment results demonstrate that the IIR GRAPPA method outperforms the current GRAPPA method by effectively suppressing noise and aliasing artifacts. The source of this improvement is the IIR inverse filter given in Eq. 6.

In Chen et al. (11,17), complete mathematical derivation and analysis of the IIR GRAPPA are provided for the one-dimensional case with $R_b = R_a = H_a = H_b = 0$. These results carry over easily to the 2D case presented

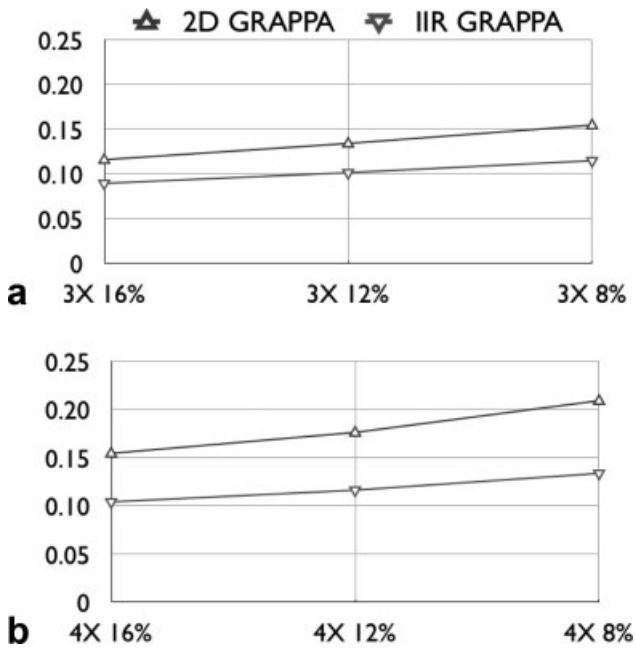

FIG. 6. Comparison of reconstruction errors of 2D GRAPPA and IIR GRAPPA with different acceleration factors and percentage of ACS lines. **a**: Three-fold acceleration and (**b**) 4-fold acceleration.

above. Discussed below are the necessity and advantages of IIR GRAPPA from three aspects: systems theory, statistical analysis, and optimization.

From the systems theory viewpoint, an optimal inverse operator Ψ must achieve perfect inversion of the imaging process and downsampling operation given in Eq. 3. Such an optimal Ψ is generally in the form of IIR and can have an FIR structure if and only if Eq. 3 is equivalent to a unimodular oversampled filter bank (11,17,24,25). For the parallel MRI system, this unimodular condition in general cannot be assumed; hence, the optimal Ψ_l should generally be IIR.

From a statistical analysis point of view, the closer two points in *k*-space, the stronger the correlation of the *k*-space data $s_l(k_y, k_x)$ at these two points. Therefore, the surrounding *k*-space data carry more information concerning an unacquired datum than those farther away and should contribute to the estimation even if they themselves are estimated. This is the central concept of AR that is theoretically and practically proven to be effective and is widely used in practice (23). This can be further understood from the pattern of $c_l(k_y, k_x)$, the convolution kernel in Eq. 3. The magnitudes of $c_l(k_y, k_x)$ are much larger in a small area around the origin than in other regions. This indicates that the adjacent data points in the convolution output $s_l(k_y, k_x)$ are highly correlated. Hence, when estimating an unacquired datum, one should make use of all surrounding data points, even if these are estimated, rather than rely on only the acquired ACS data, which may be relatively distant. As seen from Eq. 6 and Fig. 1, the data points in AR terms can be much closer to the interpolant than those in MA terms and hence more correlated with it, especially at high acceleration rates. This is clearly evidenced from the experimental results: a large-size MA term in 2D GRAPPA does not reduce much reconstruction error since it only includes more acquired data, which are farther away from and hence less correlated with the interpolant. In contrast, a small-size AR (IIR) term in IIR GRAPPA does make a considerable difference since it includes the estimated data which are closer to and hence more correlated with the interpolant.

From an optimization point of view, the IIR inverse filters with both AR (IIR) and MA coefficients belong to the solution set that includes FIR filters as a subset. Therefore, the proposed IIR GRAPPA method searches for the optimal inverse filter in a larger solution set and achieves a better performance than the conventional GRAPPA methods, which are confined to the subset of FIR solutions. Iterative GRAPPA methods (26,27) have recently shown improved image quality compared with traditional GRAPPA by iteratively searching a better FIR reconstruction filter using the reconstructed data, whereas the IIR GRAPPA approach uses IIR reconstruction filters to capture the correlation between the unacquired data points. The iterative approach can also be combined with IIR GRAPPA to search iteratively a better IIR reconstruction filter. Such a combination can potentially further improve the image quality in parallel MRI.

The reconstruction quality of GRAPPA methods also depends on the size and geometry of the receiver coils. This paper demonstrates the advantage of IIR GRAPPA using relatively large coils. In the situations of small coils or the coils being very close to the object, the k-space correlation tends to spread over a larger region. To represent such correlation, the reconstruction filter needs to have longer memory in the k_x and k_y directions. In traditional GRAPPA, this longer memory can be provided only by a larger kernel size of the FIR reconstruction filter, while in IIR GRAPPA, it can be provided by a larger kernel size of the FIR part, as well as the long memory of the IIR part. Because the IIR part has infinite memory, it has the potential to provide the long memory required for capturing the wider spread of correlations in *k*-space. Further, the benefit of including an IIR part still holds in these situations because it captures the significant correlations surrounding the unacquired points, which are absent in the traditional GRAPPA methods. It is evidenced in the implementation of IIR GRAPPA using a 32-channel head coil, where IIR GRAPPA outperforms GRAPPA reconstructions with appropriate filter sizes.

The image quality improvement in IIR GRAPPA is achieved at the expense of slightly increased reconstruction time because only a few extra coefficients are estimated. However, if reconstruction time is crucial, a reduction in FIR kernel size can be used to compensate the computation time introduced by the IIR kernel. This is evidenced from Fig. 2. Alternatively, the computationally efficient hybrid-space implementation of GRAPPA can be used (28). The hybrid-space methods transform the coefficients into image domain and then perform reconstruction. The proposed IIR framework can also be implemented in this way since the frequency response (image pixel intensities) of a discrete IIR filter is well defined and can be readily calculated. Different from the FIR situation where the DFT can be used directly for the conversion, the conversion for IIR filter should use the transfer function matrix of the filter to obtain the (complex valued) frequency response matrices in the image domain. The details of this implementation are beyond the scope of this paper and will be presented elsewhere.

Stability is important when a signal of infinite length is filtered by an IIR filter. If the IIR filter is unstable, the filter output will diverge or oscillate as the number of updates approaches infinity. However, in contrast to this type of applications, the aim of the IIR inverse filter in Eq. 6 is to minimize the sum of squares of reconstruction errors of a limited number of output values. The input to the filter always has a limited length, and hence the number of updates in the filtering operation is always limited. Therefore, the stability of an image reconstruction is less important than the accuracy of the reconstruction. If the reconstruction error produced by an inverse filter is large, we will always need reconsider the parameters or structure of the filter regardless of its stability.

Nevertheless, to guarantee the reconstruction stability, the filtering process can always be reversed for the unstable poles to form a stable noncausal filter. This is a valid procedure because the length of reconstructed data is always limited (29). Alternatively, stability-constrained estimation of IIR filter coefficients can be used to guarantee the stability.

CONCLUSION

Built upon the analysis results of Chen et al. (11,17), this paper has introduced a 2D IIR model of inverse filter to

replace the FIR model currently used in GRAPPA class methods. The proposed model captures more precisely the correlation of *k*-space data points and approximates more closely the perfect inversion of parallel imaging process, resulting in a novel generalized image reconstruction method for accelerated parallel MRI. This new reconstruction method includes conventional GRAPPA class methods as special cases and has a new IIR data estimation mechanism for effective improvement of image quality. The experiments on in vivo MRI data have shown that the proposed method significantly reduces reconstruction errors compared with GRAPPA, particularly at the higher acceleration rates. Further improvements have also been observed when multislice data are used to fit a three-dimensional spatial or spatial + temporal IIR inverse filter. The results will be reported elsewhere.

APPENDIX

Least Squares Parameter Estimation With Truncated SVD Regularization

Equation 6 can be written in the matrix form

$$\mathbf{s}_{lm} = \mathbf{\Phi}_{lm}\mathbf{G}_{lm}, \qquad [A1]$$

where $\mathbf{s}_{lm}$ is a vector containing all the data for $\hat{s}_l(Mk_y - m, k_x)$, $\mathbf{\Phi}_{lm}$ is a matrix containing all the data for $\hat{s}_j(Mk_y - m - q, k_x - r)$ and $s_j(M(k_y - b), k_x - h)$, and $\mathbf{G}_{lm}$ is a vector containing all the kernel coefficients $a_{l,m}(j, q, r)$ and $g_{l,m}(j, b, h)$.

For the coefficient vector $\mathbf{G}_{lm}$, the least squares estimation with truncated SVD regularization is given by

$$\mathbf{G}_{lm} = \sum_{i=1}^{X} \frac{1}{\sigma_i} u_i^H \mathbf{\Phi}_{lm} v_i, \qquad [A2]$$

where σ_i, u_i and v_i are obtained from the SVD of $\mathbf{\Phi}_{lm}$ given as

$$\mathbf{\Phi}_{lm} = \sum_{i=1}^{Y} u_i \sigma_i v_i^H, \qquad [A3]$$

σ_i are the singular values of $\mathbf{\Phi}_{lm}$ satisfying $\sigma_i \geq \sigma_j$ for $i < j$, and $(\cdot)^H$ denotes the complex conjugate transpose.

For $X = Y$, Eq. A2 gives the standard least squares estimation. For $X < Y$, it gives the least squares estimation with truncated SVD regularization. The level of regularization is controlled by X, which is determined by neglecting the σ_i that are less than or equal to a threshold. A larger threshold means higher-level regularization, and vice versa. For more details, see Qu et al. (21) and the references therein.

REFERENCES

1. Pruessmann KP, Weiger M, Scheidegger MB, Boesiger P. SENSE: sensitivity encoding for fast MRI. Magn Reson Med 1999;42:952–962.
2. Griswold MA, Jakob PM, Heidemann RM, Nittka M, Jellus V, Wang J, Kiefer B, Haase A. Generalized autocalibrating partially parallel acquisitions (GRAPPA). Magn Reson Med 2002;47:1202–1210.
3. Kyriakos WE, Panych LP, Kacher DF, Westin CF, Bao SM, Mulkern RV, Jolesz FA. Sensitivity profiles from an array of coils for encoding and reconstruction in parallel (SPACE RIP). Magn Reson Med 2000;44:301–308.
4. Griswold MA, Jakob PM, Nittka M, Goldfarb JW, Haase A. Partially parallel imaging with localized sensitivities (PILS). Magn Reson Med 2000;44:602–609.
5. Sodickson DK, Manning WJ. Simultaneous acquisition of spatial harmonics (SMASH): fast imaging with radiofrequency coil arrays. Magn Reson Med 1997;38:591–603.
6. Jakob PM, Griswold MA, Edelman RR, Sodickson DK. AUTO-SMASH: a self-calibrating technique for SMASH imaging: SiMultaneous Acquisition of Spatial Harmonics. MAGMA 1998;7:42–54.
7. Heidemann RM, Griswold MA, Haase A, Jakob PM. VD-AUTO-SMASH imaging. Magn Reson Med 2001;45:1066–1074.
8. Griswold MA. Advanced k-space techniques. In: 2nd International Workshop on Parallel MRI, 2004.
9. Wang Z, Wang J, Detre J. Improved data reconstruction method for GRAPPA. Magn Reson Med 2005;54:738–742.
10. Blaimer M, Breuer FA, Mueller M, Seiberlich N, Ebel D, Heidemann RM, Griswold MA, Jakob PM. 2D-GRAPPA-operator for faster 3D parallel MRI. Magn Reson Med 2006;56:1359–1364.
11. Chen Z, Zhang J, Li S, Chai L. FB analysis of PMRI and its application to H infinity optimal sense reconstruction. In: 14th IEEE International Conference on Image Processing volume 3, 2007. p III–129–III–132.
12. Griswold MA, Breuer F, Blaimer M, Kannengiesser S, Heidemann RM, Mueller M, Nittka M, Jellus V, Kiefer B, Jakob PM. Autocalibrated coil sensitivity estimation for parallel imaging. NMR Biomed 2006;19:316–324.
13. Goldfarb JW. The SENSE ghost: field-of-view restrictions for SENSE imaging. J Magn Reson Imaging 2004;20:1046–1051.
14. Griswold MA, Kannengiesser S, Heidemann RM, Wang J, Jakob PM. Field-of-view limitations in parallel imaging. Magn Reson Med 2004;52:1118–1126.
15. Breuer FA, Kellman P, Griswold MA, Jakob PM. Dynamic autocalibrated parallel imaging using temporal GRAPPA (TGRAPPA). Magn Reson Med 2005;53:981–985.
16. Huang F, Akao J, Vijayakumar S, Duensing GR, Limkeman M. k-t GRAPPA: a k-space implementation for dynamic MRI with high reduction factor. Magn Reson Med 2005;54:1172–1184.
17. Chen Z, Zhang J, Chai L. Parallel MR image reconstruction using IIR FB. In: 4th IEEE International Symposium on Biomedical Imaging: From Nano to Macro 2007. p 129–132.
18. Oppenheim AV, Schafer RW, Buck JR. Discrete-time signal processing. 2nd edition, International, Prentice Hall; 1999.
19. Kholmovski EG, Samsonov AA. GARSE: generalized autocalibrating reconstruction for sensitivity encoded MRI reconstruction from arbitrary *k*-space sampling. In: 13th Annual Meeting of the International Society for Magnetic Resonance in Medicine 2005. p 2672.
20. Hoge WS, Brooks DH. On the complimentarity of SENSE and GRAPPA in parallel MR imaging. In: 28th Annual International Conference IEEE Engineering in Medicine and Biology Society, 2006. p 755–758.
21. Qu P, Wang C, Shen GX. Discrepancy-based adaptive regularization for GRAPPA reconstruction. J Magn Reson Imaging 2006;24:248–255.
22. Nana R, Zhao T, Heberlein K, LaConte SM, Hu X. Cross-validation-based kernel support selection for improved GRAPPA reconstruction. Magn Reson Med 2008;59:819–825.
23. Ljung L. System identification: theory for the user. 2nd edition. Upper Saddle River, NJ: Prentice Hall PTR; 1999.
24. Chai L, Zhang J, Zhang C, Mosca E. Frame-theory-based analysis and design of oversampled filter banks: direct computational method. IEEE Trans on Signal Processing 2007;55:507–519.
25. Cvetkovic Z, Vetterli M. Oversampled filter banks. IEEE Trans Signal Processing 1998;46:1245–1255.
26. Zhao T, Hu X. Iterative GRAPPA (iGRAPPA) for improved parallel imaging reconstruction. Magn Reson Med 2008;59:903–907.
27. Lustig M, Pauly J. Iterative GRAPPA: a general solution for the GRAPPA reconstruction from arbitrary *k*-space sampling. In: 15th Annual Meeting of the International Society for Magnetic Resonance in Medicine, 2007.
28. Brau A, Beatty P, Skare S, Bammer R. Comparison of reconstruction accuracy and efficiency among autocalibrating data-driven parallel imaging methods. Magn Reson Med 2008;59:382–395.
29. Chen X, Zhang C, Zhang J. Error analysis of the anticausal realization of periodic inverse systems. Circuits, systems, and signal processing. http://www.springerlink.com/content/64r47g17726h2724/.